

Waves Transmission and Generation in Turbine Stages in a Combustion-Noise Framework

M. Leyko*

SNECMA, 77550 Moissy-Cramayel, France - CERFACS, 31057 Toulouse, France

S. Moreau †

GAUS, Faculté de Génie, Université de Sherbrooke, Canada

F. Nicoud‡

Université Montpellier II, 34095 Montpellier, France

T. Poinsot§

Institut de Mécanique des Fluides de Toulouse, 31400 Toulouse, France

Extended abstract

I. Introduction

A non-negligible part of the noise emitted from aero-engines is due to combustion. The relative importance of this source is even expected to increase with the next generations of engines where both fan and jet noise are reduced with such technologies as chevrons, micro-jets or highly-swept and leaned composite blades. In his PhD. dissertation,¹ Candel showed that the noise due to combustion in aero-engines could have two different origins: (a) the well-known direct combustion noise,² which is directly generated by the unsteady combustion, and transmitted and reflected through the upstream (compressor) and downstream (turbine) turbo-machinery stages; and (b) an additional source of noise, the indirect combustion noise. The latter comes from the conversion of entropy spots generated by the combustion into acoustic waves when they accelerate in the downstream turbine stages. Candel¹ showed that this source could be important and explain the observed excess noise. More recently, Leyko *et al.*³ developed scaling laws from a simplified one-dimensional (1-D) model of combustor, which showed that the indirect combustion noise could even be ten times as important as the direct one.

For both direct and indirect noise sources, the downstream turbo-machinery is involved in the transmission and generation of the combustion noise. Thus, the acoustic behavior of the turbine blade rows must be known to evaluate the noise due to combustion at the engine outlet. More specifically, the transfer functions of the turbo-machinery stages for the waves involved in the combustion process (acoustic, entropy and vortical) must be calculated. Several analytical and semi-analytical approaches have been proposed for 2-D flows to deal with the propagation of acoustic waves and vortices through turbo-machinery stages. Muir^{4,5} dealt with the case of the actuator disk theory which assumed a 2-D configuration with an infinitely thin blade row, and used classical conservation laws to establish relations between upstream and downstream flow. Kaji and Okazaki^{6,7} proposed the semi-disk actuator theory assuming in a first step that the spacing between the blades was infinitely thin but the chord-length was finite. A second step^{6,7} proposed a model with a finite chord-length and a finite spacing between blades. For both cases, the equations were solved numerically. Many other models are available for such 2-D problems. Recently Posson and Roger⁸ proposed a three-dimensional rectilinear cascade model both for generation and transmission losses based on Glegg's response,⁸ which also accounted for cascade effects and finite chord, but neglected flow deviation (flat plates

*PhD Student, email: leyko@cerfacs.fr.

†Professor, AIAA Associate Fellow.

‡Professor.

§Research Director, AIAA Associate Fellow.

at zero angle of incidence). A generalization of this model to an annular cascade is also presented in a joint paper.⁹ Literature is clearly less abundant when entropy waves are involved. Pickett¹⁰ proposed relations based on linearized equations of continuity, momentum, energy, state and second law of thermodynamics to treat entropy waves to handle turbine blade rows. Stow and Dowling¹¹ studied circumferential modes in choked nozzles. Cumpsty and Marble¹² have developed a model that takes into account entropy in the wave transmission and generation within a set of blade rows. Cumpsty and Marble¹² have generalized the 1-D model of Marble and Candel¹³ to a two-dimensional (2-D) configuration. These two models assume that the nozzle (or the blade row) is compact for the waves (the involved wavelengths are large compared with the nozzle length, or axial dimension of the blade row). Mühlbauer *et al.*¹⁴ and Leyko *et al.*¹⁵ have simulated the Entropy Wave Generator experimental configuration of Bake *et al.*,¹⁶ and have reproduced the measured indirect noise quite well. Leyko *et al.*¹⁵ have also shown that the 1-D theory of Marble and Candel¹³ works very well for this nozzle configuration, and it could help designing future experimental set-ups.

However, no experimental or numerical study has been performed to investigate indirect noise for a 2-D flow within a blade row. What is proposed in the present study is thus to look at the theoretical aspects of this model and to assess its validity by comparing with dedicated numerical results. The theoretical aspects of the model of Cumpsty and Marble¹² are first outlined in Sec. II, whereas the propagation of entropy, vorticity (because of the two-dimensional flow) and acoustic waves through an isolated blade is addressed with a Large-Eddy-Simulation (LES) code in Sec. III. Finally, the results are presented in Sec. IV and conclusions about the validity of the model are drawn in Sec. V.

II. Theory

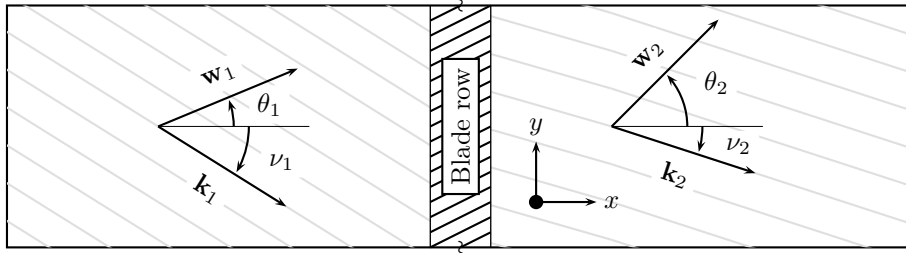


Figure 1. Schematic diagram of the flow upstream (1) and downstream (2) of the blade row in the model.¹² w is the velocity vector and k is the wave vector.

The model of Cumpsty and Marble¹² is based on the same principles as the compact nozzle of Marble and Candel,¹³ but it assumes a 2-D configuration to take into account the circumferential component of the turbo machinery and the flow deflection inducing vorticity fluctuations. Yet, the radial component of the flow is neglected (valid for large hub-to-tip ratio). The primitive variables considered here are the pressure p , the mass-density ρ , the relative velocity magnitude w and the flow orientation angle θ . The model assumes that the blade row is axially compact and that the blades spacing is small compared to the chord. The steady flows on both sides of the blade row are assumed to be different, but uniform, so that the former is treated as a planar interface, as shown in Fig. 1. Assuming that the perturbations within the flow are small, first-order balance equations relating the fluctuations (primed variables) on both sides of the blade row can be written, and the outgoing waves can be evaluated as a function of the ingoing ones and of the main characteristics of the flow (Mach number \mathcal{M} , deviation angle θ , etc.).

Since the blade row is assumed to be compact, fluctuations of entropy, mass-flow and energy are the same on both sides. For small perturbations, the conservation of the entropy between the inlet and the outlet of the blade row leads to:

$$\left(\frac{p'}{\gamma\bar{p}}\right)_1 - \left(\frac{\rho'}{\bar{\rho}}\right)_1 = \left(\frac{p'}{\gamma\bar{p}}\right)_2 - \left(\frac{\rho'}{\bar{\rho}}\right)_2 \quad (1)$$

where (1) relates to the inlet of the blade row and (2) to its outlet. For small perturbations, the mass-flow rate conservation can be expressed as:

$$\left(\frac{\rho'}{\bar{\rho}}\right)_1 + \frac{1}{\mathcal{M}_1} \left(\frac{w'}{c}\right)_1 - \theta'_1 \tan \bar{\theta}_1 = \left(\frac{\rho'}{\bar{\rho}}\right)_2 + \frac{1}{\mathcal{M}_2} \left(\frac{w'}{c}\right)_2 - \theta'_2 \tan \bar{\theta}_2 \quad (2)$$

where $\bar{\mathcal{M}}$ is the steady Mach number based on the steady velocity magnitude \bar{w} and the steady speed of sound \bar{c} . The total temperature T_t (representing the total fluid energy) is based here on the velocity magnitude w . Therefore, considering that T_t is conserved through a stator vane row yields for small perturbations:

$$\frac{1}{1 + \frac{1}{2}(\gamma - 1)\bar{\mathcal{M}}_1^2} \left[\frac{\gamma}{\gamma - 1} \left(\frac{p'}{\gamma \bar{p}} \right)_1 - \frac{1}{\gamma - 1} \left(\frac{\rho'}{\bar{\rho}} \right)_1 + \bar{\mathcal{M}}_1 \left(\frac{w'}{c} \right)_1 \right] = \dots$$

$$\frac{1}{1 + \frac{1}{2}(\gamma - 1)\bar{\mathcal{M}}_2^2} \left[\frac{\gamma}{\gamma - 1} \left(\frac{p'}{\gamma \bar{p}} \right)_2 - \frac{1}{\gamma - 1} \left(\frac{\rho'}{\bar{\rho}} \right)_2 + \bar{\mathcal{M}}_2 \left(\frac{w'}{c} \right)_2 \right] \quad (3)$$

The axial flow upstream and downstream of the blade row is here considered to be always subsonic (like in aero-engines), therefore there are always three waves traveling downward (acoustic, entropy and vorticity) and one traveling upward (acoustic). Four waves are entering the blade row (three at the inlet and one at the outlet) and four are also outgoing (one at the inlet and three at the outlet). For the flow deviation, the Kutta condition proposed by Cumpsty and Marble¹² is used:

$$\theta'_2 = \beta \theta'_1 \quad (4)$$

where β is a constant real number defined experimentally. Finally, Eqs. (1), (2), (3) and (4) can be written with the matrix $[\mathbf{E}_p^e]$ that relates the primitive variables fluctuations at the inlet and the outlet of the blade row:

$$[\mathbf{E}_p^e]_1 \cdot \begin{Bmatrix} p'/\gamma \bar{p} \\ \rho'/\bar{\rho} \\ w'/c \\ \theta' \end{Bmatrix}_1 = [\mathbf{E}_p^e]_2 \cdot \begin{Bmatrix} p'/\gamma \bar{p} \\ \rho'/\bar{\rho} \\ w'/c \\ \theta' \end{Bmatrix}_2 \quad (5)$$

with:

$$[\mathbf{E}_p^e]_1 = \begin{bmatrix} 1 & -1 & 0 & 0 \\ 0 & 1 & \frac{1}{\bar{\mathcal{M}}_1} & -\tan \theta_1 \\ \mu_1 \frac{\gamma}{\gamma - 1} & -\mu_1 \frac{1}{\gamma - 1} & \mu_1 \bar{\mathcal{M}}_1 & 0 \\ 0 & 0 & 0 & \beta \end{bmatrix} \quad (6)$$

and:

$$[\mathbf{E}_p^e]_2 = \begin{bmatrix} 1 & -1 & 0 & 0 \\ 0 & 1 & \frac{1}{\bar{\mathcal{M}}_2} & -\tan \theta_2 \\ \mu_2 \frac{\gamma}{\gamma - 1} & -\mu_2 \frac{1}{\gamma - 1} & \mu_2 \bar{\mathcal{M}}_2 & 0 \\ 0 & 0 & 0 & 1 \end{bmatrix} \quad (7)$$

where $\mu = 1/[1 + (\gamma - 1)\bar{\mathcal{M}}^2/2]$. The first line in Eqs. (6) and (7) corresponds to entropy, the second to mass-flow, the third to energy, and the last to the Kutta condition. As the experimental value of β is not available it has been set here to 10^{-6} to prevent a singular matrix.

The fluctuations of the primitive variables need to be related to the possible excitation waves (acoustic, entropy and vortical fluctuations). As the steady flows upstream and downstream of the blade row are assumed to be uniform, harmonic fluctuations (in time and space) are solutions of the underlying linearized equations (mass, momentum and entropy):

$$\frac{D}{Dt}(\rho') = -\bar{\rho} \left(\frac{\partial u'}{\partial x} + \frac{\partial v'}{\partial y} \right) \quad (8)$$

$$\frac{D}{Dt}(u') = -\frac{1}{\bar{\rho}} \frac{\partial p'}{\partial x} \quad (9)$$

$$\frac{D}{Dt}(v') = -\frac{1}{\bar{\rho}} \frac{\partial p'}{\partial y} \quad (10)$$

$$\frac{D}{Dt}(s') = 0 \quad (11)$$

where Eq. (8) is related to mass, Eqs. (9) and (10) to momentum and Eq. (11) to entropy balance equations written for small perturbations. The operator D/Dt is the substantial derivative after linearization and can be written as follows:

$$\frac{D}{Dt} = \frac{\partial}{\partial t} + \bar{u} \frac{\partial}{\partial x} + \bar{v} \frac{\partial}{\partial y} = i\omega - \bar{u}ik_x - \bar{v}ik_y \quad (12)$$

with:

$$\bar{u} = \bar{w} \cos \bar{\theta} \quad \text{and} \quad \bar{v} = \bar{w} \sin \bar{\theta} \quad (13)$$

The general form of a perturbation ϕ' can be written $\phi \exp \{-i(\omega t - \mathbf{k} \cdot \mathbf{x})\}$ where ω is the angular frequency and t the time. \mathbf{x} is the position vector (x, y) and \mathbf{k} is the wave vector that is associated with the propagation of these perturbations. This vector has an axial (k_x) and a circumferential (k_y) component defining the angle ν (see Fig. 1), therefore, the different fluctuations have a spiralling propagation. First, the entropy wave w^S is directly related to the dimensionless entropy fluctuation s'/c_p , and can be written as:

$$w^S = \frac{s'}{c_p} = A_s \exp \{-i(\omega t - \mathbf{k}_s \cdot \mathbf{x})\} \quad (14)$$

where c_p is the specific heat at constant pressure. The subscript (s) stands for quantites related to entropy perturbations. The entropy wave w^S , by definition, does not generate any velocity or pressure fluctuation. Since $s'/c_p = p'/\gamma\bar{p} - \rho'/\bar{\rho}$, the related fluctuations of primitive variables are therefore:

$$\left| \begin{array}{l} (p'/\gamma\bar{p})_s = 0 \\ (\rho'/\bar{\rho})_s = -w^S \\ (w'/c)_s = 0 \\ (\theta')_s = 0 \end{array} \right. \quad (15)$$

The entropy wave vector \mathbf{k}_s verifies the dispersion equation:

$$K_s \bar{\mathcal{M}} \cos(\nu_s - \bar{\theta}) = 1 \quad (16)$$

with $K_s = k_s \bar{c}/\omega$ the non-dimensionnal wave number. Secondly, the vorticity wave w^V is written as follows:

$$w^V = \frac{\xi'}{\omega} = A_v \exp \{-i(\omega t - \mathbf{k}_v \cdot \mathbf{x})\} \quad (17)$$

where $\xi' = \partial v'/\partial x - \partial u'/\partial y$ is the vorticity perturbation. The subscript (v) stands for quantites related to vorticity. Taking the derivative over x of Eq. (10) and subtracting the derivative over y of Eq. (9) leads to the vorticity perturbation governing equation:

$$\frac{D}{Dt} (\xi') = 0 \quad (18)$$

yielding the dispersion equation for the vorticity wave vector \mathbf{k}_v :

$$K_\xi \bar{\mathcal{M}} \cos(\nu_v - \bar{\theta}) = 1 \quad (19)$$

with $K_\xi = k_v \bar{c}/\omega$ the non-dimensionnal wave number. By noticing that the vorticity wave is divergence free, the fluctuations of primitive variables can then be related to the vorticity wave w^V :

$$\left| \begin{array}{l} (p'/\gamma\bar{p})_v = 0 \\ (\rho'/\bar{\rho})_v = 0 \\ (w'/c)_v = -i \sin(\nu_v - \bar{\theta})/K_\xi w^V \\ (\theta')_v = i \cos(\nu_v - \bar{\theta})/(K_\xi \bar{\mathcal{M}}) w^V \end{array} \right. \quad (20)$$

Thirdly, the acoustic wave propagating downward w^+ and the upward propagating one w^- are defined with respect to the related non-dimensionnal pressure fluctuations $(p'/\gamma\bar{p})_\pm$ as:

$$w^\pm = \left(\frac{p'}{\gamma\bar{p}} \right)_\pm = A_\pm \exp \{-i(\omega t - \mathbf{k}_\pm \cdot \mathbf{x})\} \quad (21)$$

where the subscript (\pm) stands for quantities related to acoustic perturbations, propagating downward (+) or upward (-). The governing equation for acoustic pressure fluctuations can be obtained as a classical wave equation:

$$\left(\frac{D}{Dt}\right)^2 (p') - \bar{c}^2 \left(\frac{\partial^2}{\partial x^2} + \frac{\partial^2}{\partial y^2}\right) (p') = 0 \quad (22)$$

yielding the dispersion equation for the acoustic wave vectors \mathbf{k}_\pm :

$$(1 - K_\pm \bar{\mathcal{M}} \cos(\nu_\pm - \bar{\theta}))^2 - K_\pm^2 = 0 \quad (23)$$

with $K_\pm = k_\pm \bar{c}/\omega$ the non-dimensionnal wave numbers. By expressing u' and v' from the momentum relations Eqs. (9) and (10), and noticing that $\rho'/\bar{\rho} = p'/\gamma\bar{p}$ when considering acoustics only, the fluctuations of primitive variables can be related to the acoustic waves w^\pm :

$$\begin{cases} (p'/\gamma\bar{p})_\pm &= w^\pm \\ (\rho'/\bar{\rho})_\pm &= w^\pm \\ (w'/c)_\pm &= K_\pm \cos(\nu_\pm - \bar{\theta}) / \{1 - K_\pm \bar{\mathcal{M}} \cos(\nu_\pm - \bar{\theta})\} w^\pm \\ (\theta')_\pm &= K_\pm \cos(\nu_\pm - \bar{\theta}) / \{\bar{\mathcal{M}} (1 - K_\pm \bar{\mathcal{M}} \sin(\nu_\pm - \bar{\theta}))\} w^\pm \end{cases} \quad (24)$$

The contribution of all waves (s , v and \pm) are summed to yield the total fluctuations of the primitive variables, since the so-called waves are independent to first-order. Equations (15), (20) and (24) are used to build the transformation matrix $[\mathbf{P}_w^p]$, which expresses the fluctuations of the primitive variables as a function of the waves:

$$\begin{pmatrix} p'/\gamma\bar{p} \\ \rho'/\bar{\rho} \\ w'/c \\ \theta' \end{pmatrix} = [\mathbf{P}_w^p] \cdot \begin{pmatrix} w^S \\ w^V \\ w^+ \\ w^- \end{pmatrix} \quad (25)$$

with:

$$[\mathbf{P}_w^p] = \begin{bmatrix} 0 & 0 & 1 & 1 \\ 1 & 0 & 1 & 1 \\ 0 & -i \frac{\sin(\nu_v - \bar{\theta})}{K_\xi} & \frac{K_+ \cos(\nu_+ - \bar{\theta})}{1 - K_+ \bar{\mathcal{M}} \cos(\nu_+ - \bar{\theta})} & \frac{K_- \cos(\nu_- - \bar{\theta})}{1 - K_- \bar{\mathcal{M}} \cos(\nu_- - \bar{\theta})} \\ 0 & i \frac{\cos(\nu_v - \bar{\theta})}{K_\xi \bar{\mathcal{M}}} & \frac{K_+ \sin(\nu_+ - \bar{\theta})}{\bar{\mathcal{M}} \{1 - K_+ \bar{\mathcal{M}} \cos(\nu_+ - \bar{\theta})\}} & \frac{K_- \sin(\nu_- - \bar{\theta})}{\bar{\mathcal{M}} \{1 - K_- \bar{\mathcal{M}} \cos(\nu_- - \bar{\theta})\}} \end{bmatrix} \quad (26)$$

The two systems of Eqs. (5), (25) can then be combined to relate the ingoing and outgoing waves respectively.

III. Numerical simulations

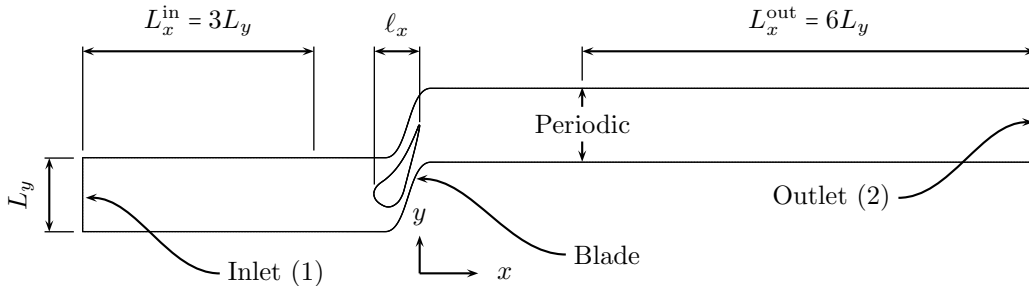


Figure 2. Description of the computational case.

The aim of the numerical simulations is to calculate the actual transfer function of a turbine stator impinged by different perturbations, in order to evaluate the error made when using the simplified compact model of Cumpsty and Marble.¹² However, computing the turbulent flow field in the complete annular blade rows of an actual turbine even at a mean radius (2-D), is still out of reach. Indeed validating the

model involves a very large range of characteristic times (ratio in the order of 10^7 in this case). On the one hand, wavelengths of the imposed perturbations have to be sufficiently large to be able to verify the compact blade row assumption. On the other hand, the time-step of the computation has to be sufficiently small to solve the flow correctly for the small geometrical details, such as the trailing-edge for instance. The simulations are therefore done for a single 2-D stator passage as the computational domain, with periodic boundary conditions on each side of the vane to mimic the infinite blade row. This limits the comparison to longitudinal waves only. Yet, circumferential waves associated with the present stator vane are only cut-on beyond 16 kHz which is out interest for the present study. The 2-D flow is simulated using the unsteady compressible LES solver AVBP.¹⁷ These Large-Eddy Simulations are performed using the Smagorinsky subgrid-scale model. The numerical scheme used for the simulations is TTG4A initially proposed by Quartapelle and Selmin.¹⁸ TTG4A scheme is third-order in space and fourth-order in time, which exhibits quite good dispersion properties. The topology of the computational case is sketched in Fig. 2. The mesh contains 115000 triangles and the origin of the reference frame is located at the blade trailing edge. The transfer functions are evaluated by only pulsating one kind of wave (entropy, acoustic or vorticity) at the computational domain boundaries (only inlet for the moment), whereas all the other in-going waves are set to zero. Only planar waves are considered and with a purely axial wave vector. The pulsed waves are imposed in the following form:

$$f(t) = \sum_{k=1}^{N_k} A_k \sin(k 2\pi t/\tau_0) \quad (27)$$

where N_k is the number of frequencies which are pulsed (50 in the present case) and where τ_0 is a fundamental characteristic period based on the frequency $f_0 = 100$ Hz ($\tau_0 = 1/f_0$). The amplitude A_k is the same for each frequency k , and it is in the order of 10^{-3} . According to Tab. 1, four kinds of simulations are performed, which starts from a statistically converged unperturbed flow. The simulations with perturbations of entropy (S-1), vorticity (V-1) and acoustic (A-1) waves at the inlet provide the acoustic-to-acoustic, the vorticity-to-acoustic and entropy-to-acoustic transfer functions of the blade row, whereas the simulation N-0 evaluates the global noise level, to verify that it is lower than the one produced by the perturbation of the inlet waves. For simulations S-1, V-1 and A-1, the frequencies of the imposed signal are representative of what can be found at the outlet of a real combustion chamber (not detailed in the present study).

Subsonic case: $M_1 = 0.12$, $\theta_1 = 0$ and $M_2 = 0.66$, $\theta_1 = 76^\circ$			
Name	Perturbed wave	Location	Duration
S-1	Entropy	Inlet (1)	$66 \tau_0$
V-1	Vorticity	Inlet (1)	$66 \tau_0$
A-1	Acoustic	Inlet (1)	$66 \tau_0$
A-2	Acoustic	Outlet (2)	-
N-0	None	-	$18 \tau_0$

Table 1. Description of the different simulations.

IV. Results

As shown in Fig. 3, the generalization to a 2-D configuration (blade rows) made by Cumpsty and Marble has a major effect on the propagation of both indirect (left plot) and direct noise (right plot) compared with the 1-D model of Marble and Candel. As mentioned in Sec. II, the 2-D model can deal with any angle of attack of the incident waves. The acoustic responses at the outlet of a blade row w_2^+ to a purely axial entropy perturbation at the inlet w_1^S (Fig. 3 (a)), and to an acoustic one at the inlet w_1^+ (Fig. 3 (b)) are then plotted for different inlet and outlet flow angles θ_1 and θ_2 , respectively. For the model of Marble and Candel, the Mach number based either on the total velocity magnitude or on the axial component of the velocity is used. It can be seen that the 2-D and 1-D models provide quite different results for important flow deviations, as it can be found in turbine stages. It should also stressed that for $\theta_1 = \theta_2 = 0$, the results of the two theories collapse as expected.

Several results have been obtained on the stationary stator vane sketched in Fig. 2 impacted by a parallel

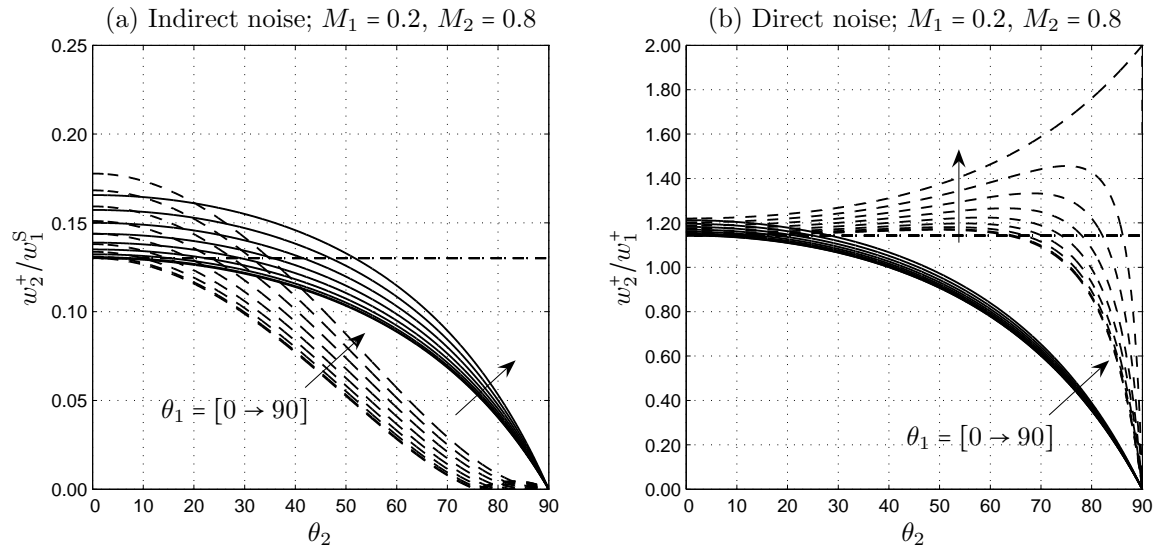


Figure 3. Acoustic response of the blade row at the outlet (2) to a perturbation at the inlet (1) for different flow directions. (a) Entropy perturbation; (b) Acoustic perturbation. Cumpsty and Marble (—), Marble and Candel with global Mach number (---), Marble and Candel with axial Mach number (- - -).

gust (normal to the blade row) of the excitations given in Tab. 1. The entropy wave remains planar before the blade row (there is no injection of vortical perturbations) and is rather perturbed after the interaction with the blade row (Reynolds number based on the chord length $Re_c \approx 10^6$). Therefore, the post-processing of the waves is performed by integration of the required quantities along the transversal direction, since the waves of interest are axially oriented ($k_y = 0$). Afterwards, quadratic averaging of the wave Fourier-transform modulus is performed along the axial direction. The local 1-D waves w_x^j , where the superscript j stands for (S), (V), (+) or (-), are thus calculated as follows:

$$w_x^j(x, k) = \left| \frac{1}{N_t \tau_0} \int_0^{N_t \tau_0} \left\{ \frac{1}{L_y} \int_0^{L_y} w^j(x, y, t) dy \right\} \exp(i2\pi f_0 k t) dt \right| \quad (28)$$

where N_t is the number of computed periods τ_0^a and L_y is the height of the inter-blade channel (see Fig. 2). The global 1-D waves w^j are obtained using the following relation:

$$w^j(k) = \sqrt{\frac{1}{L_x} \int_0^{L_x} \{w_x^j(x, k)\}^2 dx} \quad (29)$$

where L_x corresponds to $3L_y$ for the waves at the inlet (subscripted 1) and $6L_y$ for the waves at the outlet (subscripted 2) as depicted in Fig 2. The acoustic response of the blade row [acoustic waves propagating upstream (a) and downstream (b)] to an entropy perturbation plotted as a function of the frequency (simulation S-1) is shown in Fig. 4. Two values of the non-dimensionalised entropy wavelength λ/ℓ_x based on the inlet quantities are also depicted to provide an idea of the compactness of the blade row for the perturbed frequency range. The transfer function obtained from the simulation S-1 tends to the model for the low-frequencies, and decreases rapidly for higher frequencies. Figure 5 shows the acoustic response of the blade row to a downward propagating acoustic wave (simulation A-1) perturbation. The non-dimensional acoustic wavelength λ/ℓ_x is also depicted. The transfer function obtained from the simulation A-1 is thus very close to the model value since the perturbed wavelengths λ are large compared with the blade axial length ℓ_x . Finally, Fig. 6 shows the acoustic response of the blade to a vorticity perturbation (simulation V-1). The observed LES levels are actually close to those without perturbation (simulation N-0). This is then consistent with the theoretical result: the model predicts that the vorticity does not generate any acoustic wave, since the flow is axial at the blade row entrance ($\theta_1 = 0$). Therefore, the comparison is not really relevant for this particular test-case.

^a $\tau_0 = 1/f_0$ where $f_0 = 100$ Hz.

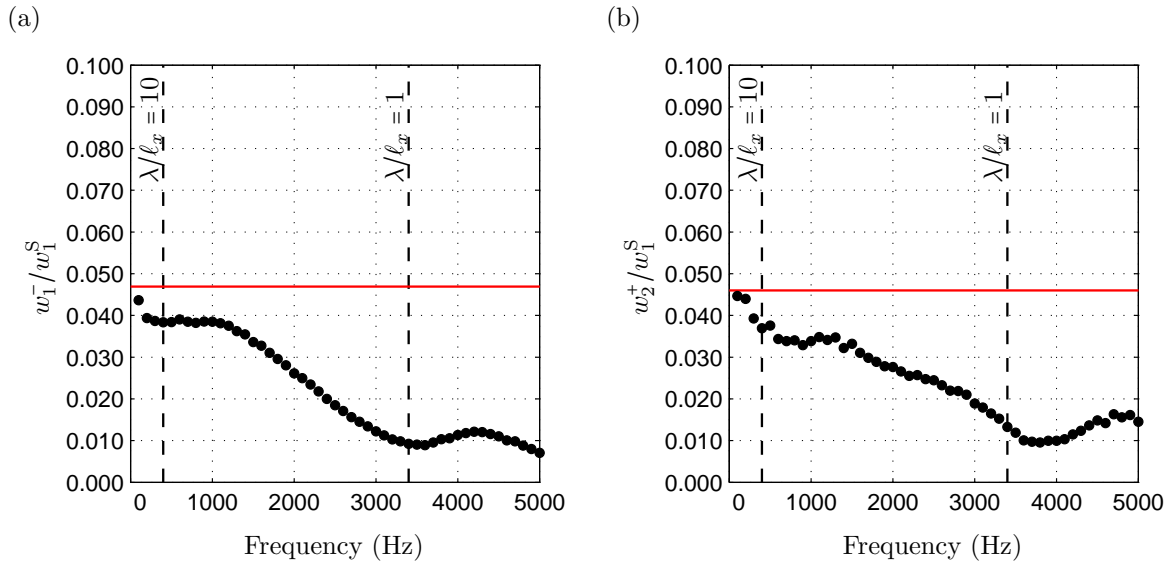


Figure 4. Acoustic response of the blade row to an entropy perturbation at the inlet (S-1). (a) Upstream propagating waves; (b) Downstream propagating waves. Model (—), simulation (●).

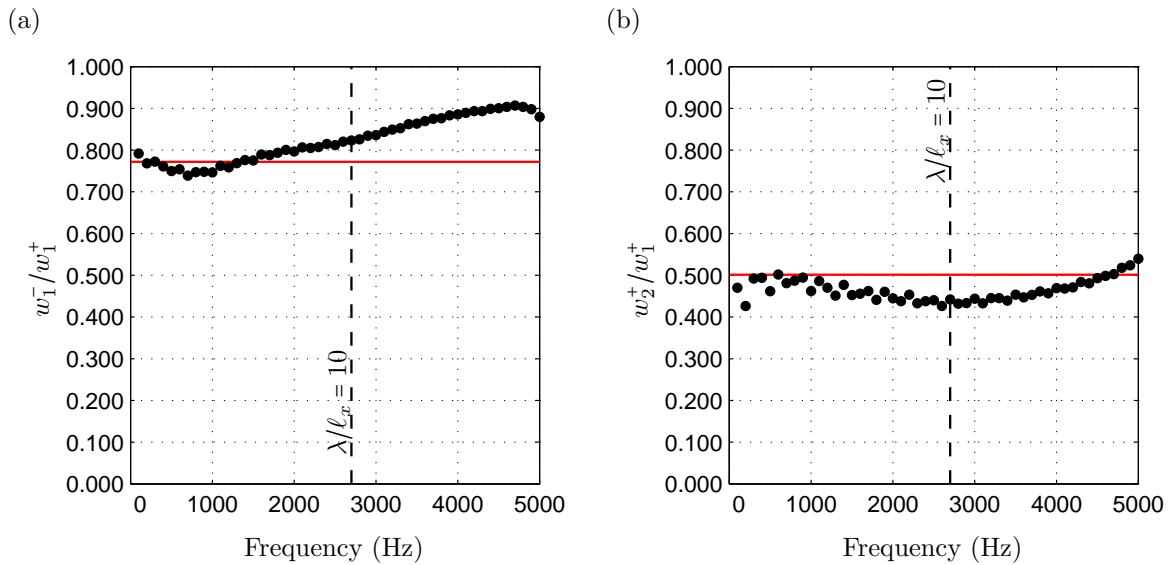


Figure 5. Acoustic response of the blade row to an acoustic perturbation at the inlet (A-1). (a) Upstream propagating waves; (b) Downstream propagating waves. Model (—), simulation (●).

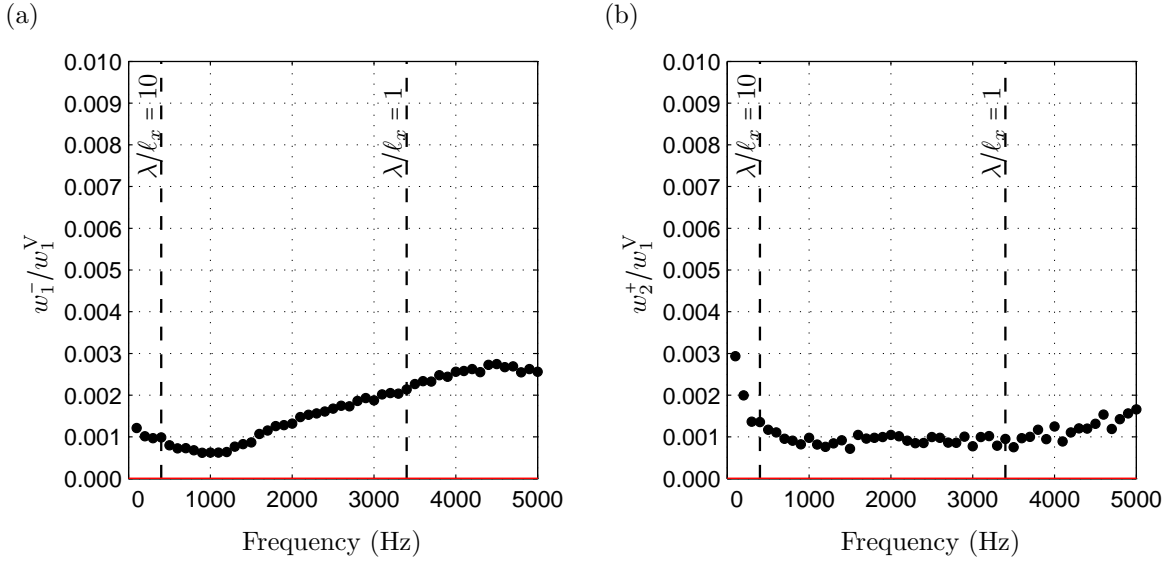


Figure 6. Acoustic response of the blade row to a vorticity perturbation at the inlet (V-1). (a) Upstream propagating waves; (b) Downstream propagating waves. Model (—), simulation (●).

As seen in Section II, the model of Cumpsty and Marble¹² assumes that the entropy is conserved. The verification of this statement can be interesting if the model is used for more than one blade row. The turbulent mixing in the flow downstream of the blade row strongly affects the structure of the wave and the initial planar coherence of the entropy perturbation is lost for higher frequencies as shown in Fig. 7 (a). The global entropy wave, as defined as the axially averaged wave (Eq. 29), is not representative in this case, since the mixing process takes place after the blade row. The evolution along the axial direction of the entropy wave is more relevant of its attenuation, described by the ratio $w_{x,2}^S/w_1^S$, and is shown in Fig. 7 (b) for different frequencies. Lower frequencies (larger wavelengths) are almost not affected by the mixing which occurs at the scales of the blade dimension, and levels remain the same until the outlet. The intensity of small wavelengths not only decreases more rapidly, but mostly the waves are already attenuated at the very beginning of the downstream section ($x/l_x = 0$). Since the spacing between the stator and the rotor Δx is generally very small ($\Delta x/l_x < 0.5$), it is interesting to understand the reasons of such a phenomenon. The attenuation in the channel between blades can be explained by the distortion of the planar waves by the steady flow, and can be calculated from the related 2-D velocity field. The distortion of the waves at the outlet of the blade row is here evaluated using lagrangian tracking of particles seeded at the inlet (post-processing of the steady flow). Figure 8 (a) shows the path-lines of the particles computed from the steady flow (the flow is quasi-steady in channel between blades), whereas Fig. 8 (b) shows particle-lines seeded at the same time. Both graphs show that the flow between the blades is not uniform. As a consequence, initially axially co-current particles have a different time of arrival at the blade row outlet plane ($x/l_x = 0$). Figure 8 (b) clearly reveals the deformation of the initially planar waves. The delay in the arrival of particles at the outlet $t_d(y)$ is plotted in Fig. 10 (a) versus the transversal direction y made non-dimensional by the pitch length L_y ($y/L_y = 0$ and $y/L_y = 1$ correspond to the blade trailing-edges). This quantity is obtained by calculating the duration required by a particle to reach the outlet plane $x/l_x = 0$ when following a given path-line. The particles passing by the trailing-edges should theoretically have an infinite time of arrival, but have a finite value here because of the finite number of path-lines used to evaluate the function $t_d(y)$. This function can be directly used to calculate the *attenuation* of the entropy waves, which no longer appear as planar at the outlet of the blade row (see for example in Fig.9 (a)). Indeed, each series of particles can be associated to a sinusoidal level of amplitude. As a consequence, the 1-D temporal fluctuations (averages along the transversal direction y) at the blade row outlet $d_0(t, k)$ can be simply expressed as follows:

$$d_0(t, k) = \frac{1}{L_y} \int_0^{L_y} \exp \{i2\pi k f_0 [t + t_d(y)]\} dy \quad (30)$$

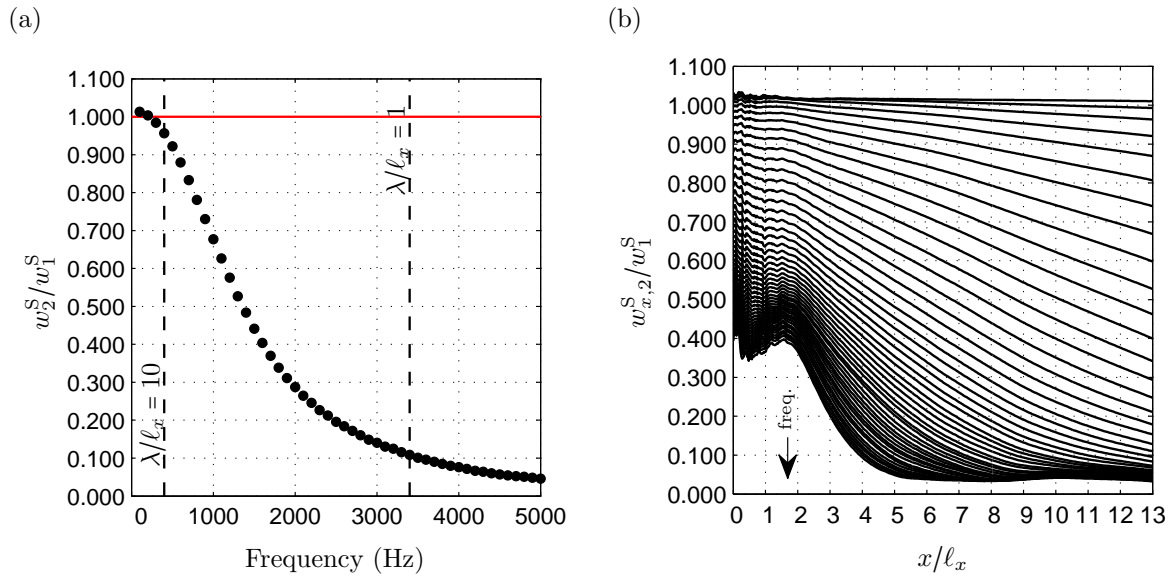


Figure 7. Entropy response of the blade row at the outlet to an entropy perturbation at the inlet. (a) Global entropy wave, where (—) stands for the model, and (●) for the simulation; (b) Local entropy wave at the outlet, where the different curves represent different frequencies.

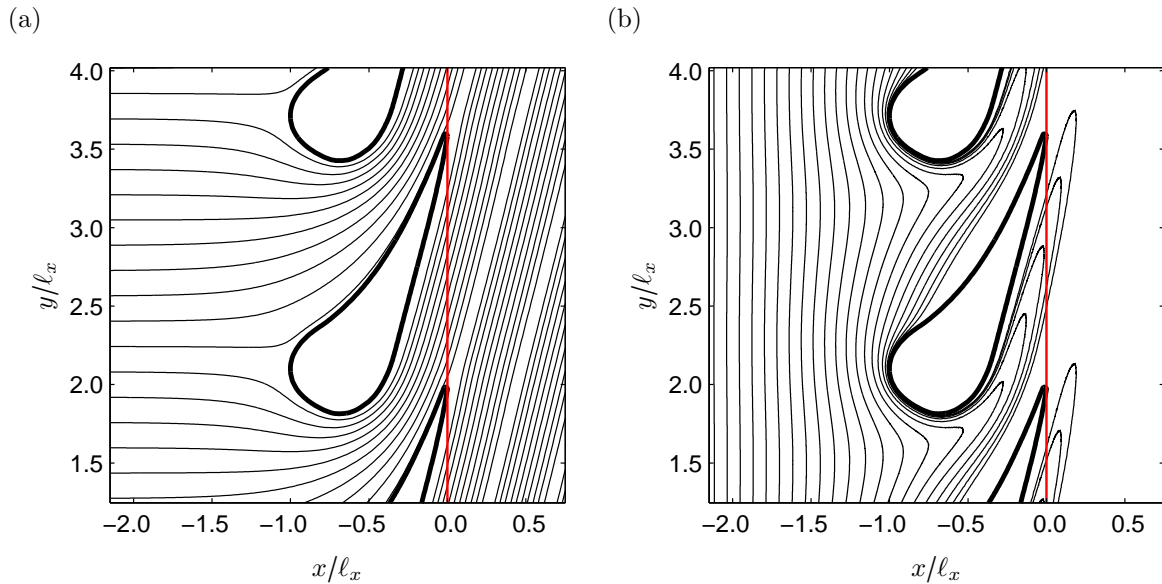


Figure 8. Mean flow characteristics. (a) Path-lines calculated from the mean flow; (b) Particles-lines seeded from the inlet and calculated from the mean flow.

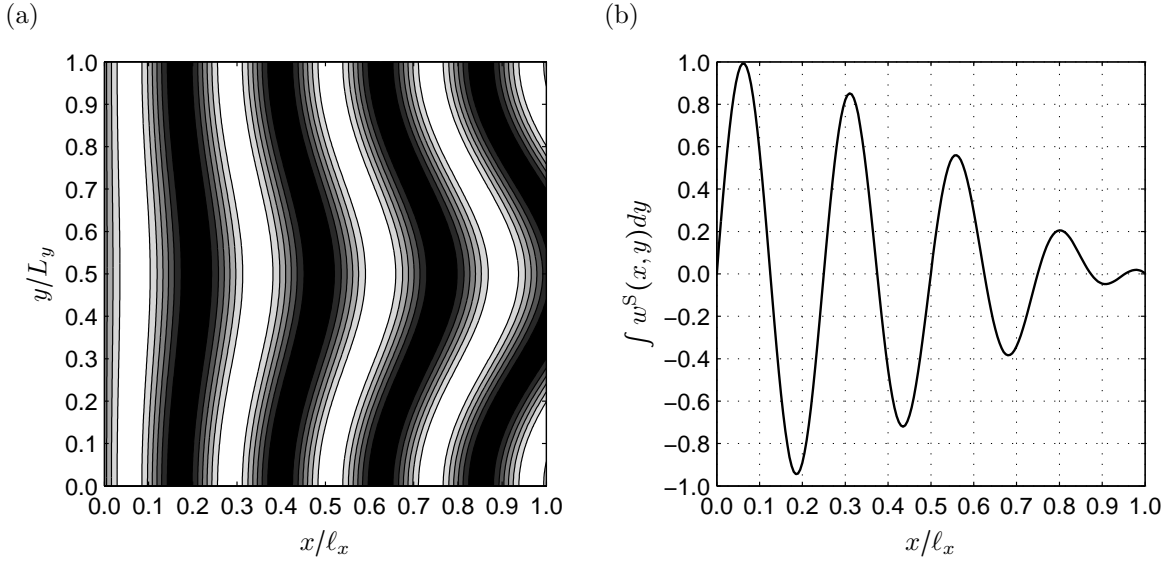


Figure 9. Example of entropy wave distortion. (a) 2-D field of entropy wave $w^S(x, y)$ with faster mean flow in the middle; (b) Integral of the entropy wave over the transversal direction y .

The local entropy fluctuations are actually not reduced, but simply redistributed in space. Using Eq. 30, the attenuation of the longitudinal waves $D_0(k)$ for the frequency k is:

$$D_0(k) = \left| \frac{1}{L_y} \int_0^{L_y} \exp \{i2\pi k f_0 t_d(y)\} dy \right| \quad (31)$$

which only depends on the function $t_d(y)$ and on k . In Fig. 10 (b) (for $n = 0$), the attenuation measured in the simulation, and the one computed using the mean flow distortion, are in a quite good agreement for almost the whole spectrum. This point strongly supports that the attenuation for small convective wavelength at the beginning of the downstream section is caused by the distortion of initially planar waves by the mean flow. It is interesting to remark that this phenomenon will of course produce non-planar waves at the outlet. A more general expression for Eq. (31) can be:

$$D_n(k) = \left| \frac{1}{L_y} \int_0^{L_y} \exp \{i2\pi [k f_0 t_d(y) + n(y/L_y)]\} dy \right| \quad (32)$$

where the integer n corresponds to the n -th transversal wave vector component related to the propagation of the entropy wave. This function is also plotted in Fig. 10 for different values of n ($n = [-3 : 3]$). One can see that when the frequency tends to zero, only planar waves ($n = 0$) are observed and without attenuation. When the wavelength diminishes (higher frequency) the transversal waves appear whereas the longitudinal wave strongly decreases (for wavelengths in the order of the blade dimension, or rather the blade spacing). These observations suggest that, to study the non-compact aspects of the propagation of entropy waves, not only planar waves should be looked at, even if the excitation is planar. This redistribution of the entropy fluctuations can have an influence when several blade rows are involved.

The model of Cumpsty and Marble¹² also predicts the generation of vorticity waves. It can be interesting to look at this aspect in the scope of the coupling between different blade rows, even if it has been seen that there is no noise theoretically caused by the vorticity in the present investigated case. Figure. 11 shows the response of the blade row in terms of vorticity to either an entropy (a), or an acoustic perturbation (b). The vorticity induced by the entropy perturbations in simulation S-1 seems to be negligible in comparison to the vorticity caused by the trailing-edge wake, and thus the model seems to under-predict the vorticity response of the blade row. This statement is confirmed by Fig. 12 that shows the vorticity levels at the inlet and the outlet of the blade row for all simulations. Concluding about the validity of the model for the induced vorticity in simulation S-1 is thus impossible since the magnitude of the imposed entropy perturbations is

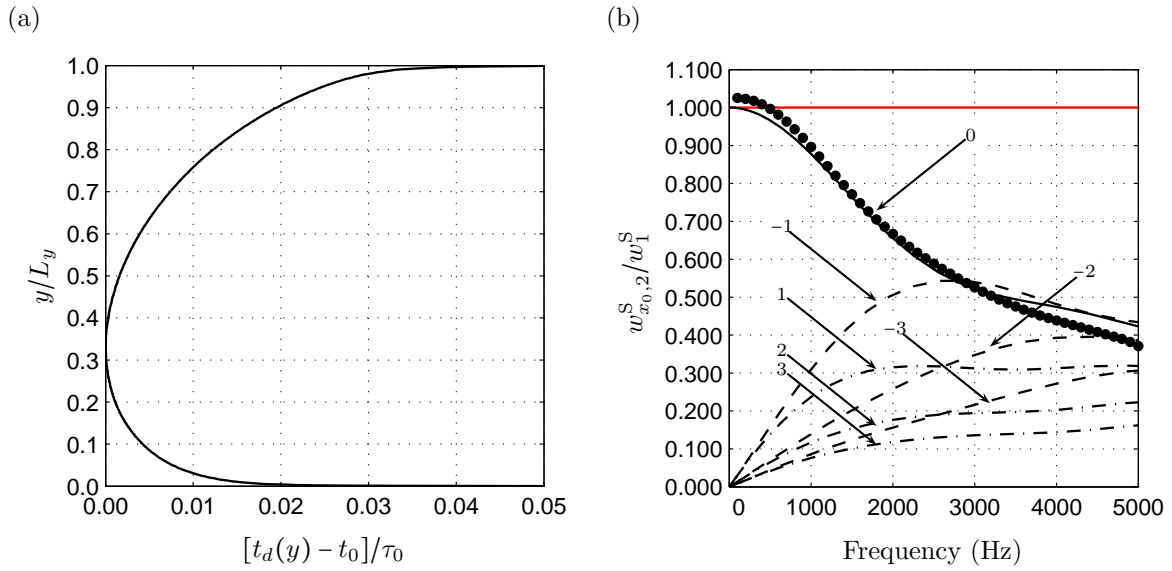


Figure 10. (a) Difference in time for a particle to reach the blade row outlet x_0 on a given path-line. (b) Attenuation $D_n(k)$ of the entropy wave through the blade row: calculated from the steady flow (—), simulated (●) for $n = 0$. From the post-processing with $n < 0$ (---) and $n > 0$ (-.-).

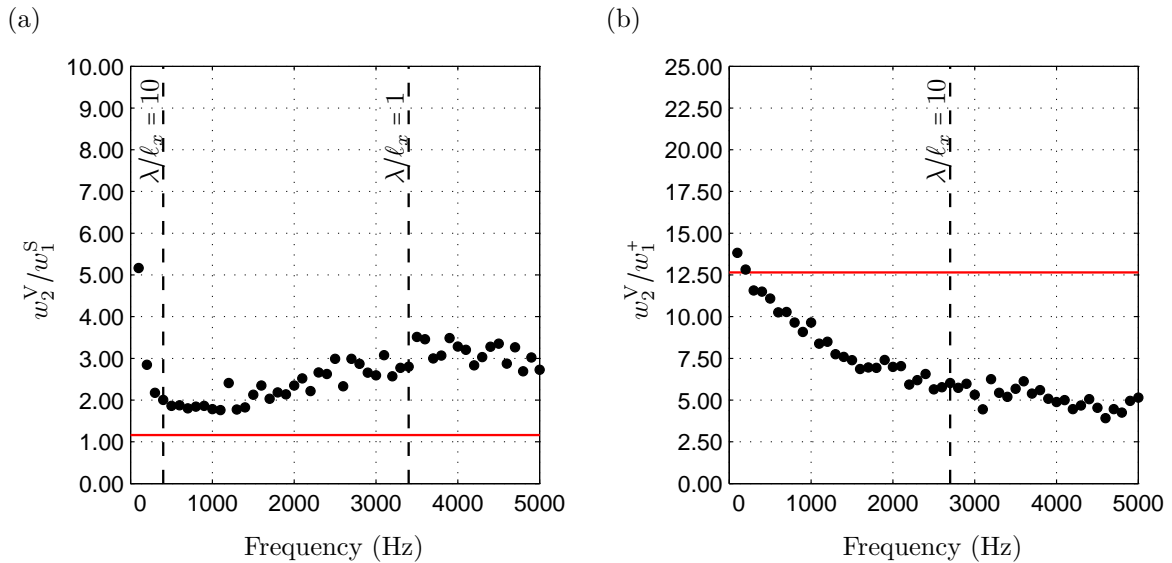


Figure 11. Vorticity response of the blade row to an entropy or acoustic perturbation at the inlet (case S-1 and A-1). (a) Entropy; (b) Acoustic. Model (—), simulation (●).

too small. However for the simulation A-1 (Fig. 11 (b)), which seems to exhibit more vorticity because of the acoustic perturbation (see Fig. 12), the model works well in the low frequency range.

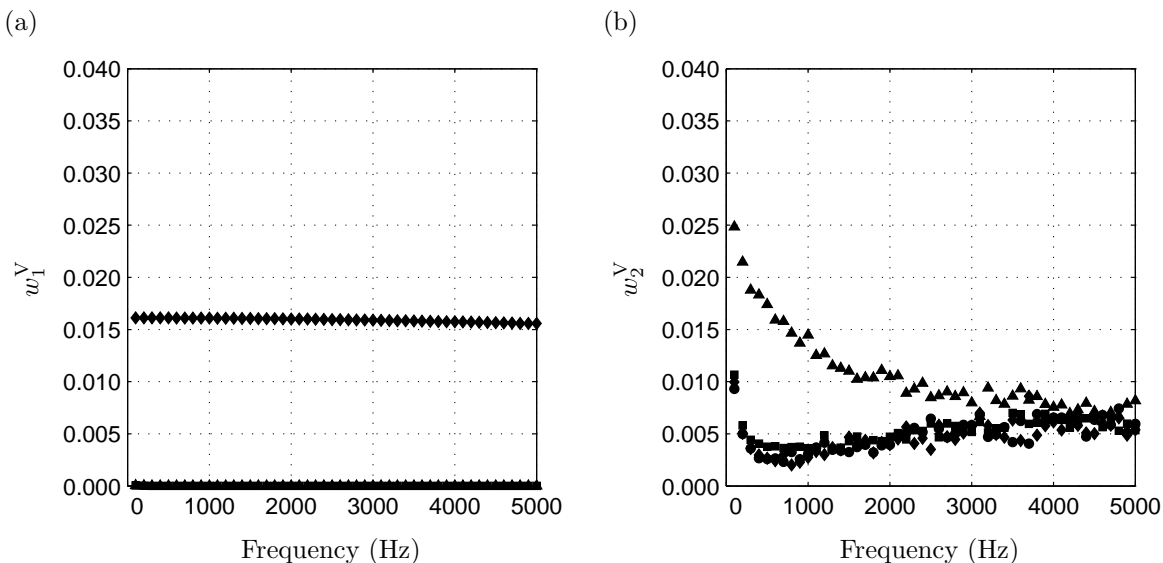


Figure 12. Vorticity at the inlet (a) and outlet (b) for the four different simulations. Simulation N-0 (\bullet), S-1 (\blacksquare), V-1 (\blacklozenge) and A-1 (\blacktriangle).

V. Conclusions

In the present study, the generalization to a 2-D configuration made by Cumpsty and Marble is shown to have a major effect on the acoustic transmission through blade rows compared with the 1-D model of Marble and Candel. The 2-D model can deal with any angle of incidence of the impinging waves, and even for incident axial ones the difference can be large. The acoustic responses at the outlet of a blade row w_2^+ to a purely axial entropy perturbation at the inlet w_1^S , and to an acoustic one at the inlet w_1^+ are found to provide quite different results for important flow deviations as found in actual turbo-machines.

Numerical unsteady simulations of the response of an isolated blade row have also been performed in a 2-D configuration to evaluate the validity of the analytical model of Cumpsty and Marble,¹² which assumes a compact blade row. The acoustic transmission and reflection is well predicted by the model in the investigated frequency range (100-5000 Hz). The acoustic waves generated by entropy disturbances impinging on the blade row is also well predicted at low-frequencies (100-500 Hz or for $\lambda/\ell_x > 10$), but the theoretical results rapidly depart from the numerical ones for higher frequencies. Moreover, a proper post-processing of the steady flow has shown that the initially planar entropy waves are also strongly distorted by the inter-blade non-uniform steady flow at high-frequencies. This last point can lead to additional disagreement when considering coupling between blade rows. However, entropy perturbations within an actual aeronautical combustion chamber are expected to be mostly in the low-frequency range. Therefore the derived transfer functions should be considered taking into account more realistic inputs coming from measurements or LES results at the exit of a combustion chamber. The calculation of the errors made on the noise prediction at the outlet of an actual distributor vane shows that an error of 0.6 dB is done on the direct noise, and 2.0 dB on the entropy one, when using the present model with disturbances spectra from an actual combustor LES. The entropy fluctuations obtained in the latter are in the low-frequency range, therefore the overall indirect noises calculated analytically and numerically are in the same range of magnitude. The results provided by this first-order approach are globally quite good and make it suitable as part of a core-noise evaluation tool.

References

- ¹Candel, S., *Analytical studies of some acoustic problems of jet engines.*, Ph.D. thesis, California Institute of Technology, Pasadena, California, 1972.
- ²Bragg, S., "Combustion noise," *Journal of Institute of Fuel*, Vol. 36, No. 264, 1963, pp. 12–16.
- ³Leyko, M., Nicoud, F., and Poinso, T., "Comparison of Direct and Indirect Combustion Noise Mechanisms in a Model Combustor," *AIAA Journal*, Vol. 47, No. 11, November 2009, pp. 2709–2716.
- ⁴Muir, R. S., "The application of a semi-actuator disk model to sound transmission calculations in turbomachinery, part I: The single blade row," *Journal of Sound and Vibration*, Vol. 54, No. 3, October 1977, pp. 393–408.
- ⁵Muir, R. S., "The application of a semi-actuator disk model to sound transmission calculations in turbomachinery, part II: Multiple blade rows," *Journal of Sound and Vibration*, Vol. 55, No. 3, Decembre 1977, pp. 335–349.
- ⁶Kaji, S. and Okazaki, T., "The application of a semi-actuator disk model to sound transmission calculations in turbomachinery, part I: The single blade row," *Journal of Sound and Vibration*, Vol. 11, No. 3, March 1970, pp. 339–353.
- ⁷Kaji, S. and Okazaki, T., "Propagation of sound waves through a blade row: II. Analysis based on the acceleration potential method," *Journal of Sound and Vibration*, Vol. 11, No. 3, March 1970, pp. 355–375.
- ⁸Posson, H. and Roger, M., "Parametric study of gust scattering and sound transmission through a blade row," *13th AIAA/CEAS Aeroacoustics Conference and Exhibit, Rome, Italy - AIAA Paper 2007-3690*, 2007.
- ⁹Posson, H., Moreau, S., Blériot, H., de l'Epine, B., and Schram, C., "Prediction of sound transmission through an annular cascade using an analytical cascade response function," *16th AIAA/CEAS Aeroacoustics Conference and Exhibit, Stockholm, Sweden - AIAA Paper 2010-4030*, 2010.
- ¹⁰Pickett, G. F., "Core engine noise due to temperature fluctuations convecting through turbine blade rows," *2nd AIAA Aeroacoustics Conference - AIAA 1975-528*, 1975.
- ¹¹Stow, S. R., Dowling, A. P., and Hynes, T. P., "Reflection of circumferential modes in a choked nozzle," *Journal of Fluid Mechanics*, Vol. 467, No. 1, 2002, pp. 215–239.
- ¹²Cumpsty, N. and Marble, F., "The interaction of entropy fluctuations with turbine blade rows; a mechanism of turbojet engine noise," *Proc. R. Soc. Lond.*, Vol. 357, No. 1690, Novembre 1977, pp. 323–344.
- ¹³Marble, F. E. and Candel, S., "Acoustic disturbances from gas nonuniformities convected through a nozzle," *J. Sound and Vibration*, Vol. 55, No. 2, 1977, pp. 225–243.
- ¹⁴Mühlbauer, B., Noll, B., and Aigner, M., "Numerical investigation of the fundamental mechanism for entropy noise generation in aero-engines," *Acta Acustica united with Acustica*, Vol. 95, 2009, pp. 470–478.
- ¹⁵Leyko, M., Nicoud, F., Moreau, S., and Poinso, T., "Numerical and analytical investigation of the indirect combustion noise in a nozzle," *Comptes Rendus Mécanique*, Vol. 337, No. 6-7, 2009, pp. 415–425.
- ¹⁶Bake, F., Richter, C., Mühlbauer, B., Kings, N., Röhle, I., Thiele, F., and Noll, B., "The Entropy Wave Generator (EWG): A reference case on entropy noise," *Journal of Sound and Vibration*, Vol. 326, No. 3-5, October 2009, pp. 574–598.
- ¹⁷Moureau, V., Lartigue, G., Sommerer, Y., Angelberger, C., Colin, O., and Poinso, T., "Numerical methods for unsteady compressible multi-component reacting flows on fixed and moving grids," *J. Comput. Phys.*, Vol. 202, No. 2, 2005, pp. 710–736.
- ¹⁸Quartapelle, L. and Selmin, V., "High-order Taylor-Galerkin methods for non-linear multidimensional problems." 1993.